

Resonant spin Hall effect in a nano-ribbon of a spin-orbit coupled electron system

Mohamad Usman,¹ Tarun Kanti Ghosh,² and SK Firoz Islam¹

¹*Department of Physics, Jamia Millia Islamia, New Delhi-110025, INDIA*

²*Department of Physics, Indian Institute of Technology-Kanpur, Kanpur-208016, INDIA*

We present a theoretical study of spin Hall phenomena in a nanoribbon made of a two-dimensional square lattice with Rashba and Dresselhaus spin-orbit coupling. We show that the nanoribbon can give rise to a number of additional spin degeneracy points as well as anti-crossing points, apart from the Γ point, between two nearest sub-bands. We compute the spin Hall conductivity and demonstrate that it diverges and gives rise to a resonance when chemical potential passes through those spin-degenerate or anti-crossing points. Contrary to the previous studies, here such resonance emerges even without any external perturbation like magnetic field or light. In addition, we examine the influence of anisotropy in Rashba and Dresselhaus interactions, as well as finite-temperature effects, and show that the inter subband resonance remains robust. Finally, we also investigate the signature of such additional spin degeneracy and anti-crossing points in the longitudinal conductance by using retarded Green function approach in lattice model. The peculiar features of the bands are reflected in the longitudinal conductance, which takes quantized values of $2ne^2/h$, where n denotes the number of bands occupied by the chemical potential with each band having spin split sub-bands.

I. INTRODUCTION

The spin Hall effect (SHE)[1–4] is the hall mark of spin-orbit coupling term in a two-dimensional (2D) fermionic system in which fermions with opposite spins are scattered to opposite transverse edge normal to the applied bias. The spin-orbit interaction is the result of relativistic effect, and in a 2D electronic system it mainly arises due to inversion symmetry breaking field across the semiconductor heterojunctions[5, 6]. There are two types of spin-orbit interactions, namely Rashba spin-orbit interaction (RSOI) and Dresselhaus spin-orbit interaction (DSOI). The RSOI arises due to the lack of structural inversion symmetry across the quantum well in a semiconductor heterojunction [7], whereas the DSOI is the result of bulk inversion symmetry breaking [8]. The RSOI is externally tunable by applying a gate voltage [9–11], whereas the DSOI is an intrinsic property of the system that cannot be enhanced or tuned through external perturbations. The spin-orbit interaction removes the spin-degeneracy even in the absence of a magnetic field. Typical materials that exhibit RSOC include indium-based compounds such as InAs and heterostructures like GaInAs/GaAlAs. The degree of spin separation along the transverse direction to the applied bias is generally quantified by spin Hall conductivity (SHC) that was predicted to exhibit a universal constant value in 2D electron gas (2DEG) with k -linear RSOC[2]. Subsequently, the SHC in a 2D heavy-hole gas (2DHG) with k -cubic RSOI was also carried out and found that instead of universal constant value it's sensitive to the strength of RSOI[14, 15].

Apart from the above mentioned works on SHE, usual integer quantum Hall phenomena in such spin-orbit coupled system were also carried out [16–21]. A series of theoretical investigations on spin-related transport phenomena in 2DHG in presence of weak magnetic field have also been studied[22–25]. Moreover, the search for the materials or mechanisms to achieve giant or large SHC[26–28] continues to be an active topic in the field of spintronics.

It is noteworthy to mention that the SHE is one of the key signatures of spin-Hall edge modes in the quantum-spin-Hall liquid discovered in 2D Dirac materials with spin-orbit coupling[29, 30]. The key difference with quantum spin-Hall insulator is that it belongs to \mathbb{Z}_2 topological insulator where bulk is insulating gapped with counter propagating spin-dependent gapless edge modes. Whereas in semiconductor heterostructures, the SHE is not associated with topology and its bulk is neither gapped nor it is due to spin-dependent edge modes. The SHE in semiconductor heterostructure is purely due to momentum dependent spin sensitive Lorentz force aided by spin-orbit interaction. From the experimental perspective, semiconductor compounds are still much more reliable platform than 2D Dirac materials to realize SHE.

The present work is motivated by the phenomena called spin Hall resonance based on spin-orbit coupled quantum Hall system, predicted by Shen. *et al.* [31], in which the spin Hall conductivity exhibits a resonance if spin splitting vanishes between two nearest Landau levels with opposite spin at chemical potential. Such resonance was also predicted in a cubic Rashba system [32]. Recently, one of us has shown that even without Landau level such resonance can occur by applying linearly polarized light, in a k -cubic Rashba system [33]. In this work, our objective is to seek an answer of the question- is it possible to achieve such resonance even without any external perturbations like magnetic field or light? We show that such resonance can occur between two nearest sub-bands with opposite spin in a finite-size system where the width is relatively much smaller compared to length. In fact, we note that a large number of spin-splitting vanishing points and anti-crossing points can emerge at different energy ranges among the higher sub-bands. We discretize the system on a square lattice and consider both normal-edge and zigzag-edge nanoribbons. We analyze their band spectrum and subsequently study the spin Hall conductivity in both types of nanoribbon.

This paper is organized as follows. In Sec. II, we intro-

duce the model Hamiltonian and its discretization. Section III is devoted to the band structure of the nanoribbon. The Transport properties along with the effects of anisotropy and finite temperature on the spin Hall conductivity are presented and discussed in Sec. IV. and finally, Sec. V summarizes our findings and provides concluding remarks.

II. MODEL HAMILTONIAN AND DISCRETIZATION

In this section, we briefly discuss the electronic system first. Our objective is to study the spin transport with the finite size effects in a 2D electronic system. In order to include these effects, we need to work in a real space basis by discretizing the well-known spin-orbit coupled low energy effective Hamiltonian[7]-[8]

$$H = -\frac{\hbar^2 \nabla^2}{2m^*} - i\alpha (\sigma_x \partial_y - \sigma_y \partial_x) - i\beta (\sigma_x \partial_x - \sigma_y \partial_y), \quad (1)$$

where $\partial_j = \partial/\partial j$ ($j = x, y$), α and β are the strength of the Rashba and the Dresselhaus spin-orbit interactions, $\sigma = \{\sigma_x, \sigma_y\}$ are Pauli matrices in real spin basis, and m^* is the effective mass of the electron. In order to discretise the Hamiltonian, we shall assume a square lattice with the lattice periodicity a along both the x - and y - directions. We use the plane wave representation of annihilation operator in the basis of lattice sites (j, l) , $c_{\mathbf{k}, \sigma} = \frac{4\pi^2}{a^2} \sum_{j,l} e^{-ia(k_x j + k_y l)} c_{j,l,\sigma}$, we obtain the substitution rules for the continuum momentum operators (with $\lambda = x, y$)

$$k_\lambda \mapsto \frac{1}{a} \int_{\text{BZ}} d^2 k \sin(ak_\lambda) c_{\mathbf{k}, \sigma}^\dagger c_{\mathbf{k}, \sigma} \quad (2)$$

$$k_\lambda^2 \mapsto \frac{2}{a^2} \int_{\text{BZ}} d^2 k [1 - \cos(ak_\lambda)] c_{\mathbf{k}, \sigma}^\dagger c_{\mathbf{k}, \sigma} \quad (3)$$

using the Eq. 3 in the kinetic energy operator

$$H_{kin} = \frac{\hbar^2}{2m^*} \int_{\text{BZ}} d^2 k \frac{2}{a^2} [2 - \cos(ak_x) - \cos(ak_y)] c_{\mathbf{k}, \sigma}^\dagger c_{\mathbf{k}, \sigma} \quad (4)$$

Performing the Fourier transform to real space yields

$$H_{kin} = -t \sum_{j,l,\sigma,s} \left(c_{j,l,\sigma}^\dagger c_{j+s,l,\sigma} + c_{j,l,\sigma}^\dagger c_{j,l+s,\sigma} \right) + 4t \sum_{j,l,\sigma} n_{j,l,\sigma} \quad (5)$$

where $t = \hbar^2/(2m^*a^2)$, $\sigma : \uparrow, \downarrow$, $s = \pm 1$ and $n_{j,l,\sigma} = c_{j,l,\sigma}^\dagger c_{j,l,\sigma}$. The on-site term $4t \sum_{j,l,\sigma} n_{j,l,\sigma}$ is an overall energy shift and can be omitted by redefining the zero of energy, yielding the standard nearest-neighbor tight-binding kinetic term:

$$H_{kin} = -t \sum_{j,l,\sigma,s} \left(c_{j,l,\sigma}^\dagger c_{j+s,l,\sigma} + c_{j,l,\sigma}^\dagger c_{j,l+s,\sigma} \right) \quad (6)$$

In the similar fashion, the RSOI and DSOI terms can also be represented in discrete lattice space. Using Eq. (2) in the Rashba and Dresselhaus interaction terms in Eq. (1), we obtain the second quantized form of the Rashba spin-orbit interaction [34] and Dresselhaus spin-orbit interaction [35] as

$$H_R = -\frac{i\alpha}{2a} \sum_{j,l,\sigma,\sigma',s} s \left(\sigma_x^{\sigma\sigma'} c_{j,l,\sigma}^\dagger c_{j,l+s,\sigma'} - \sigma_y^{\sigma\sigma'} c_{j,l,\sigma}^\dagger c_{j+l,\sigma'} \right), \quad (7)$$

$$H_D = -\frac{i\beta}{2a} \sum_{j,l,\sigma,\sigma',s} s \left(\sigma_x^{\sigma\sigma'} c_{j,l,\sigma}^\dagger c_{j+l,\sigma'} - \sigma_y^{\sigma\sigma'} c_{j,l,\sigma}^\dagger c_{j+l+s,\sigma'} \right), \quad (8)$$

The full tight-binding Hamiltonian including kinetic energy and both the SOC contributions is thus

$$H = H_{kin} + H_R + H_D. \quad (9)$$

III. ENERGY SPECTRUM OF THE NANORIBBON

Having established the tight-binding Hamiltonian in real space and its discretization on a square lattice, we now turn to the nanoribbon geometry, which is the central focus of this work. In particular, we analyze two types of nanoribbons, namely straight-edge and zigzag-edge geometries as shown in Fig. 1(a) and Fig. 1(b), respectively. To obtain the energy spectrum for nanoribbons with both types of edge terminations, we construct a Hamiltonian analogous to the infinite lattice case [36, 37]. We define a nanoribbon as a stripe of finite width along the x -direction whereas infinitely extended along the y -direction. Because of the translational symmetry and lattice periodicity along the y -direction, we can write down the total Hamiltonian by using Bloch's theorem as

$$H = H_{00} + H_{10} e^{ik_y a} + H_{-10} e^{-ik_y a}, \quad (10)$$

where H_{00} is the on-site hopping matrix including the spin-orbit coupling of each supercell as highlighted in red colour in Fig. 1, and H_{10} denotes the hopping matrix between two nearest supercells. The width of the ribbon is described by the number of atomic sites in each supercell. Note that because of the translational symmetry along the y -direction, k_y is a conserved quantity and acts as a good quantum number. The energy eigen values are computed numerically by diagonalizing Eq. (10). The tight-binding Hamiltonian, including spin degrees of freedom, yields $2N$ energy sub-bands.

We plot energy spectrum for zigzag nanoribbon in presence of RSOI and DSOI in Fig. (2). For better visualisation, the energy spectrum is shown only for a few lowest sub-bands around the Γ point. The energy spectrum is referenced from a baseline value of $4t$, which corresponds to a constant energy shift applied to the full Hamiltonian. The straight edge band spectrum is given in the

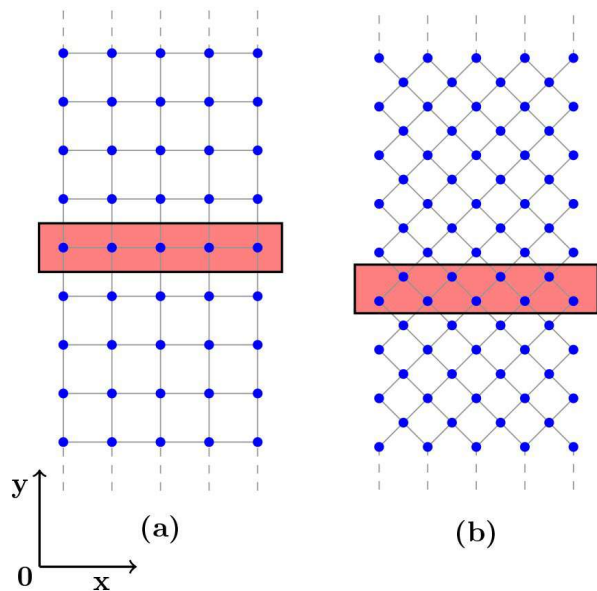


FIG. 1: Schematic plots of (a) straight edge nanoribbon of a square lattice, and (b) zigzag edge nanoribbon of square lattice. The unit cell is shown by the rectangular region highlighted by red colour.

Appendix, as its qualitative features are essentially the same.

In the bulk, spin degeneracy is guaranteed at the Γ point, and we find that this characteristic is preserved in the nanoribbon, with all sub-bands remaining spin-degenerate at Γ point. In addition, several extra spin degeneracy points where the spin splitting vanishes emerge within the same sub-band. Moreover, number of spin degeneracy points as well as anti-crossing points appear between two nearest sub-bands with opposite spin at different k_y points. It is important to note that anti-crossing points are distinct from spin degeneracy points, in the latter, the spin splitting vanishes, whereas in the former the two bands approach each other very closely but a small energy gap remains. We attribute these additional degeneracies and anticrossings to the competition between the RSOI and DSOI i.e., only Rashba or Dresselhaus alone cannot give rise to such degeneracy points and anti-crossing points. This is very much similar to the case of Rashba spin-orbit coupled quantum Hall system [31], where such additional spin-degeneracy is the result of the competition between the Rashba and Zeeman splitting. However, in the present case the Zeeman splitting is absent and its role is played by DSOI, whereas the Landau level index is played by finite width induced energy sub-bands. In zigzag-edge nanoribbon, increasing β enhances the strength of inter-band anticrossings. In particular, for $\beta = 0.09$ [Fig. 2], the spin-split sub-bands show visibly larger anticrossings, whereas for smaller β the anticrossings remain relatively weak.

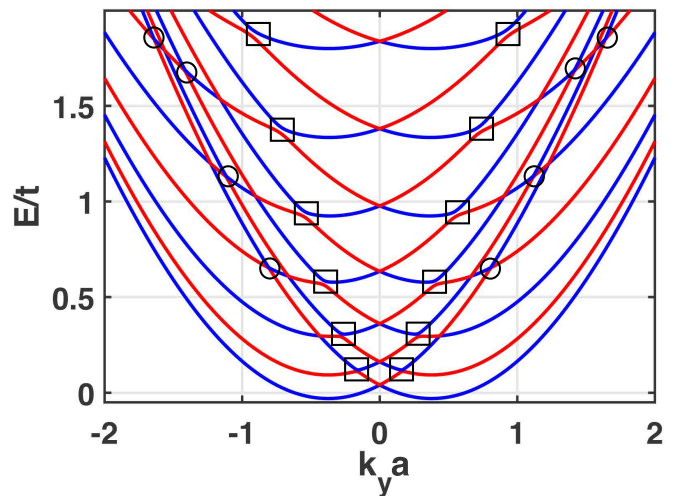


FIG. 2: Energy spectrum of zigzag edge nanoribbon for $\alpha = 0.1$ and $\beta = 0.09$ in units of ta . The red and blue curves denote spin-up and spin-down branches. The anti-crossings and spin-degeneracy between two nearest sub-bands are shown by squares and circles, respectively.

IV. TRANSPORT PROPERTIES OF THE NANORIBBON

A. Spin Hall conductivity

The spin Hall conductivity is calculated by using linear response based Kubo formula as used in Ref.[2]. However, in the nanoribbon case, the system is infinite along the y direction and preserves the translational symmetry, whereas the width is restricted along the x -direction breaking the translational symmetry. Hence, k_y remains the conserved quantity and acts as a good quantum number. Hence an electronic state can be fully described by $\zeta = \{s, k_y, n\}$ where n is the sub-band index and $s = +(-)$ denotes spin-up (down). The SHC can now be written for a nanoribbon as

$$\sigma_{xy}^z = \frac{e\hbar}{\Omega} \sum_{\zeta \neq \zeta'} (f_{\zeta} - f_{\zeta'}) \frac{\text{Im} [\langle \zeta | \hat{J}_x^z | \zeta' \rangle \langle \zeta' | \hat{v}_y | \zeta \rangle]}{(E_{\zeta'} - E_{\zeta})^2}, \quad (11)$$

where $\Omega = L_x \times L_y$ denotes the area, $f_{\zeta} = [1 + \exp\{(E_{\zeta} - \mu)/(k_B T)\}]^{-1}$ is the Fermi-Dirac distribution function with μ being the chemical potential. Also, \hat{J}_x^z is the spin current operator and is given by $\hbar\{\sigma^z, \hat{v}_x\}/4$, where the velocity operators are obtained $\hat{v}_y = (\hbar)^{-1} \partial H / \partial k_y$ and $\hat{v}_x = (i\hbar)^{-1} [H, x]$ with $x = \sum_n c_n^\dagger n c_n$ [38]. In the above Eq. 11 we perform $\sum_{\zeta \neq \zeta'} \rightarrow (L_y/2\pi) \int dk_y \sum_{n, n', s, s'}$ to calculate the SHC for the nanoribbon geometry.

We evaluate the SHC for zigzag nanoribbon and straight edge nanoribbons. The zigzag case is shown in the Fig. 3 whereas the straight edge is not shown here rather shifted to appendix A as qualitative nature remain same. We observe that the SHC is enhanced sharply

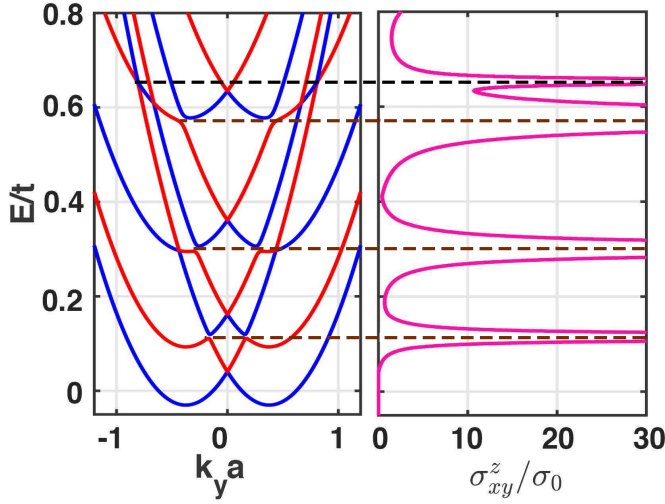


FIG. 3: Band structure (left) and spin Hall conductivity normalized with $\sigma_0 = e/(8\pi)$ for a zigzag edge nanoribbon with width $N = 21$ and $\alpha = 0.1$, $\beta = 0.09$ in units of ta at temperature $k_B T/t = 10^{-5}$. The SHC exhibits resonance at various μ . The brown dashed lines highlight the resonance due to interband anti-crossings, while the black dashed lines indicate the resonance due to vanishing spin splitting.

at a number of chemical potential, which correspond to the inter-band spin splitting vanishing or anti-crossing points. This enhanced peaks are nothing but the so-called spin Hall resonance which precisely occur at the energies corresponding to the inter-band spin degeneracy points or anti-crossing points in the band structure. Importantly, we also check that in the limiting cases of a pure Rashba system ($\beta = 0$) or a pure Dresselhaus system ($\alpha = 0$), the inter-band spin degeneracy points are strongly suppressed or absent, and as a result, the SHC does not exhibit any resonant peaks. This observation suggests that a relative competition between two types of spin-splitting is required to achieve such resonance, here it is caused by RSOI and DSOI.

Our findings resonate well with the theoretical predictions made by Shen *et al.* [31], where they studied resonant spin Hall conductance in 2DEGs under a perpendicular magnetic field. In that work, the RSOI competes with the Zeeman splitting to induce energy level crossings that give rise to the resonance. In our case, an analogous mechanism takes place in nanoribbons via the interplay between RSOI and DSOI, resulting in anti-crossings and degeneracy points between spin-resolved sub-bands and subsequent enhancement of the SHC.

It is noteworthy to mention that when $\alpha = \beta$, the system exhibits a high degree of symmetry, and although many anti-crossings are visible in the band structure, the matrix elements of the spin current operator vanishes. Consequently, the SHC is identically zero across the entire range of chemical potentials. We also comment that as the spin Hall phenomena occurs in a 2D

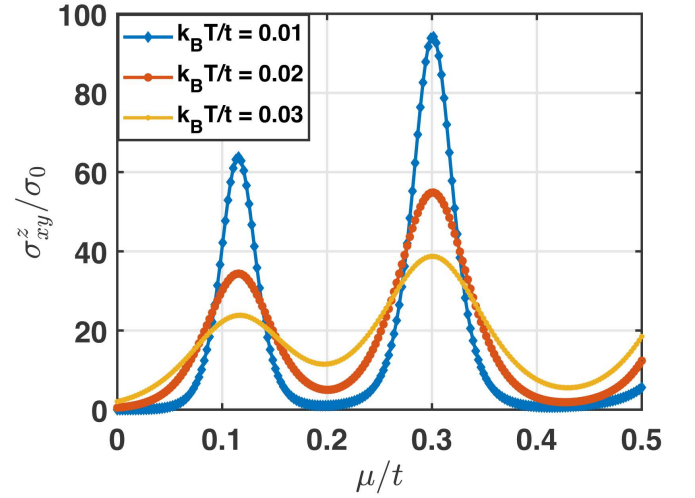


FIG. 4: Spin Hall conductivity versus chemical potential for zigzag edge nanoribbon with width $N = 21$ and $\alpha = 0.1$, $\beta = 0.09$ in units of ta for various temperatures.

fermionic system, it is desirable to keep width also quite large compared to the present case. Here, we keep width very narrow as $N = 21$ only to make degeneracy or anti-crossing points clearly visible. With the further increase of width a large number of sub-bands will be formed and many such degeneracy or anti-crossing points exhibiting resonance in SHC will occur.

Next, we briefly discuss the spin Hall phenomena in a 2D electronic system with an anisotropic RSOI and DSOI. The ab-initio calculation based theoretical prediction in the surface states of $Au(110)$ suggested the existence of an anisotropic Rashba splitting [39]. In fact the C_{2v} point-group symmetry analysis not only suggested the mass anisotropy but also hinted an anisotropic RSOI [40] as $H_R = \alpha_x k_x \sigma_y + \alpha_y k_y \sigma_x$ where $\{\alpha_x, \alpha_y\}$ are two independent parameters describing the degree of spin splitting along two orthogonal directions in momentum space. Similarly, anisotropic Dresselhaus interaction can be modeled as $H_D = \beta_x k_x \sigma_x - \beta_y k_y \sigma_y$ with $\{\beta_x, \beta_y\}$ denoting the anisotropy in the DSOI. These generalization naturally extend the isotropic case and allow us to investigate the robustness of SHR under reduced lattice symmetry. In the discrete lattice model, such anisotropy can be captured by considering a weak imbalance between hopping parameters along two orthogonal directions as t_x and t_y , as $t_y = \nu t_x$ where ν describes the degree of anisotropy. Following the same approach as in the isotropic Rashba–Dresselhaus case, we compute both the band structure and the corresponding SHC, and note that the spin degeneracy points and the anti-crossing points persist even in the presence of anisotropy. The SHC continues to exhibit resonance whenever the chemical potential lies at these points. It indicates that inter sub-bands resonance phenomena in spin Hall conductivity is robust to weak anisotropy in band structure.

We now turn to the role of finite temperature on the SHC, we find that the suppression of spin Hall conductivity at finite temperature is more pronounced at the lower energy degeneracy points compared to the higher energy ones [Fig.4]. This behavior can be understood in terms of the difference between the Fermi occupation factors. When the chemical potential lies in the lower bands, the upper band remains nearly unoccupied and hence the difference is essentially governed by the lower band Fermi function. In this regime, the thermal broadening of the Fermi function strongly reduces the SHC resonance. However, when the chemical potential is located in the higher bands, both the upper and lower bands are partially occupied. The effect of broadening then tends to cancel out between the two bands, leading to a much weaker suppression of SHC at the higher energy degeneracy and anticrossing points. Hence, we conclude that the resonance features in the higher bands are more robust to temperature effects.

Next, we briefly check whether the longitudinal transport exhibits any signatures of vanishing spin splitting or anti-crossings.

B. Longitudinal transport

The longitudinal conductivity characterizes the charge transport along the translationally invariant direction under the application of an external bias. In order to capture the contribution of finite width induced sub-bands, it is convenient to use the real space Green function based approach developed by Sancho *et al.* [41, 42]. In this approach the longitudinal direction is taken to be very long compared to the width, and both the ends of the ribbon are attached to two leads of identical system. Following this approach it is straight forward to write the transmission between two leads through central region at E as[43]

$$\mathcal{T}(E) = \text{Tr}[\Gamma_L G_{11}(E) \Gamma_R G_{11}^\dagger(E)]. \quad (12)$$

where

$$G_{11} = [(E + i\eta)I - H_{11} - \Sigma_L - \Sigma_R]^{-1} \quad (13)$$

is the retarded Green's function of the scattering region including the effects of the leads attached to both ends. The leads are encoded into the above total Green function through $2N \times 2N$ matrices $\Gamma_{L,R} = i(\Sigma_{L,R} - \Sigma_{L,R}^\dagger)$ where Σ_L and Σ_R are self energy function due to left and right lead, respectively.

At zero temperature, the longitudinal conductance follows from the Landauer-Büttiker relation[44, 45],

$$G(E) = \frac{e^2}{h} \mathcal{T}(E), \quad (14)$$

By using Eq. (12) we compute zero temperature conductance as a function of chemical potential against the

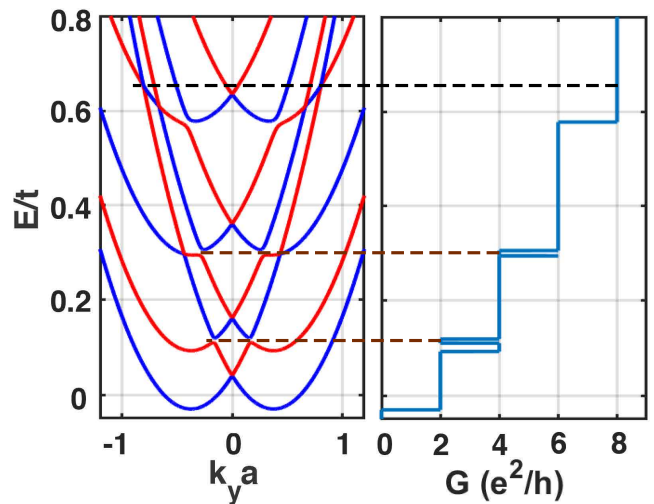


FIG. 5: Band structure (left) and corresponding longitudinal conductance (right, in units of e^2/h) for a zigzag edge nanoribbon with $\alpha = 0.1$, $\beta = 0.09$ in units of ta and the width is $N = 21$. The brown dashed lines highlight interband anti-crossings while the black dashed lines show interband spin degeneracy point.

corresponding band structure for zigzag edge nanoribbon in the Fig. 5. As usual, the conductance exhibits quantization in units of $2e^2/h$ when $\mu < 0.1$. This can be attributed to the fact that only one sub-band with two electron incident channels is occupied by the chemical potential. As the chemical potential starts occupying the spin up sub-band of the lowest sub-band, both bands contribute one incident channel each maintaining the conductance again at $2e^2/h$. At $\mu \approx 0.1$ the conductance suddenly increases to $4e^2/h$ reflecting the existence of four electron incident channels, three from the spin up sub-band and one from the spin down sub-band. However, within very a very narrow range of μ around 0.1, the conductance drops back to $2e^2/h$ and then rises again to $4e^2/h$. This unusual feature originates from the presence of an anti-crossing point at $\mu = 0.1$. With further increase in μ , the phenomenon reappears at $\mu = 0.3$ corresponding to another anticrossing point. We emphasize that such behavior does not occur at the inter-subband spin degeneracy points. Hence we can conclude that although a signature of anti-crossing point is visible in longitudinal conductance, it shows no corresponding features at the inter-band spin degeneracy. Finally, we note that the qualitative features of the conductance remain the same for the straight edge case, with the only difference being a shift in the locations of the anticrossing points.

V. SUMMARY

We have investigated the spin-Hall transport and longitudinal transport for a 2D electronic system with RSOI

and DSOI in a discrete lattice model. We have considered square lattice system with straight edge and zigzag edge geometry. In both cases, we showed that a number of spin degeneracy points and anti-crossing points between two nearest sub-band with opposite spin emerges. The spin-Hall conductivity shows a sharp enhancement when the chemical potential is situated at those spin-degeneracy points or anticrossing points, exhibiting spin-Hall resonance. Hence, we conclude that resonance in spin-Hall conductivity can be achieved without applying any external perturbation like magnetic field or light field as proposed previously. However such resonance can occur only if RSOI and DSOI both are present. We have also investigated the effects of anisotropy and finite temperature and demonstrated that the latter results in suppression of SHC but this suppression is weaker in higher energy degeneracy and anticrossing points while the former results in a shift of the position of resonance points in the spin Hall conductivity and finally we study the longitudinal conductance by using retarded Green function approach, and reveal that anti-crossing point can give a signature to the conductance whereas the degeneracy point does not leave any mark.

VI. ACKNOWLEDGEMENT

SK Firoz Islam acknowledge financial support by the project ANRF/ECRG/2024/005166/PMS.

Appendix A: Straight-edge nanoribbon: Band structure and Transport properties

We briefly discuss the case of a straight edge nanoribbon here. We present lowest few spin-split sub-bands for straight edge nanoribbon in Fig.6 where red and blue curves represent the spin-up and spin-down components, respectively. Very much similar to the case of zigzag ribbon, here also a number of spin-splitting vanishing as well as anti-crossing points are present between two nearest sub-bands, which are highlighted by circles and squares respectively. It is noticeable that the number of such points are relatively higher in straight edge case compared to zigzag edge. It is expected that the SHR can occur when the chemical potential passes through the inter sub-band spin degenerate or anti-crossing points. The SHC is plotted in the Fig. 7 showing multiple resonances.

The longitudinal conductance for straight edge ribbon is also plotted in Fig. 8 which also shows quantized steps in units of $2e^2/h$, with the overall features similar to the zigzag case.

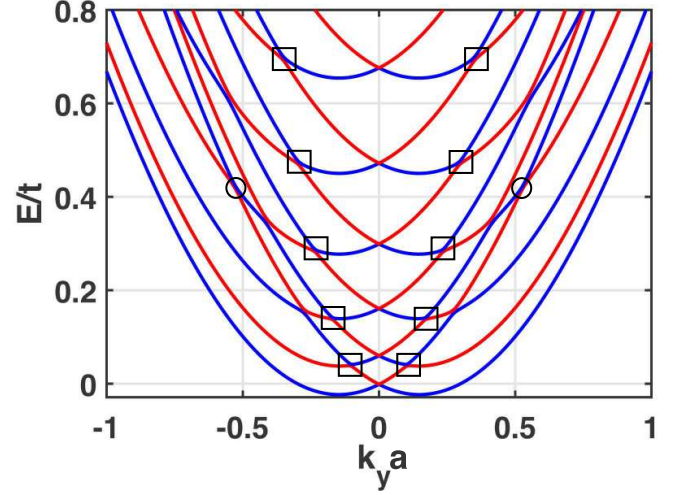


FIG. 6: Band dispersion for straight edge nanoribbon along k_y for $\alpha = 0.11$ and $\beta = 0.1$ in units of ta . Red and blue curves denote spin-up and spin-down components. The emergence of interband anticrossings and degeneracy induced by the competition between Rashba and Dresselhaus couplings are highlighted by squares and circles respectively.

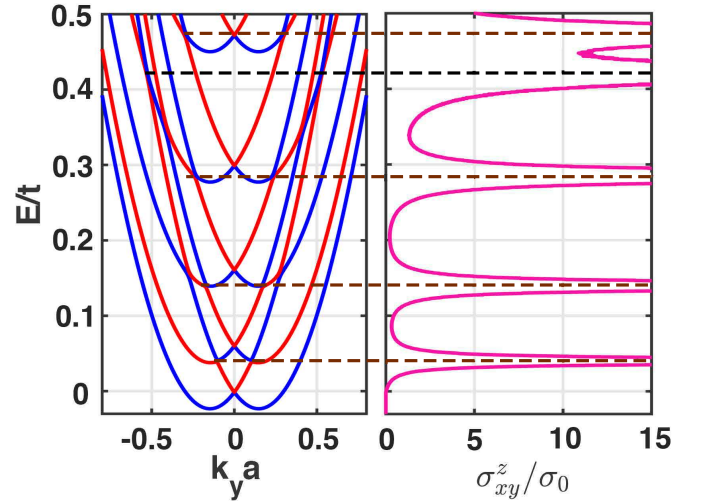


FIG. 7: Band structure (left) and corresponding spin Hall conductivity normalized with $\sigma_0 = e/8\pi$ for straight edge nanoribbon with width $N = 21$ and $\alpha = 0.11$, $\beta = 0.1$ in units of ta and the temperature $k_B T/t = 10^{-5}$. The SHC exhibits resonance at various μ . The brown dashed lines highlight the resonance due to interband anti-crossings, while the black dashed lines indicate the resonance due to vanishing spin splitting.

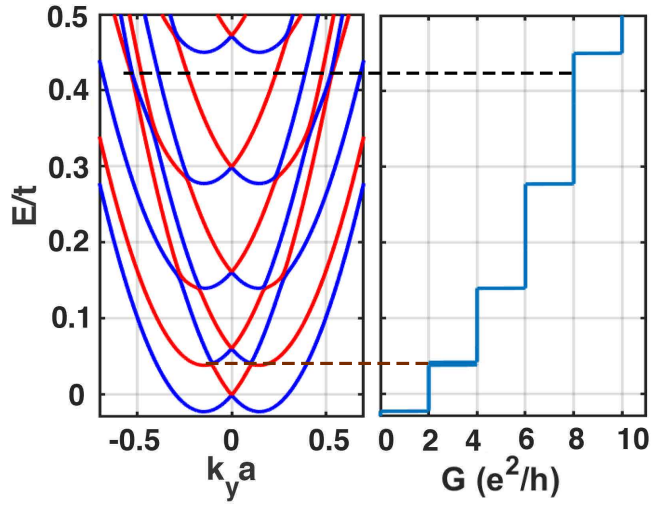


FIG. 8: Band structure (left) and corresponding longitudinal conductance (right, in units of e^2/h) for a straight edge nanoribbon with $\alpha = 0.11$, $\beta = 0.1$ in units of ta and the width is $N = 21$. The brown dashed lines highlight interband anti-crossings while the black dashed lines show interband spin degeneracy point.

-
- [1] J. E. Hirsch, Phys. Rev. Lett. **83**, 1834 (1999).
- [2] J. Sinova, D. Culcer, Q. Niu, N. A. Sinitsyn, T. Jungwirth, and A. H. MacDonald, Phys. Rev. Lett. **92**, 126603 (2004).
- [3] J. Sinova, S. O. Valenzuela, J. Wunderlich, C. H. Back, and T. Jungwirth, Rev. Mod. Phys. **87**, 1213 (2015).
- [4] S. Murakami, N. Nagaosa, and S.-C. Zhang, Science **301**, 1348 (2003).
- [5] R. Winkler, *Spin-Orbit Coupling Effects in Two-Dimensional Electron and Hole Systems*, Springer Tracts in Modern Physics, Vol. 191 (Springer, 2003).
- [6] I. Žutić, J. Fabian, and S. Das Sarma, Rev. Mod. Phys. **76**, 323 (2004).
- [7] Y. A. Bychkov and E. I. Rashba, JETP Lett. **39**, 78 (1984).
- [8] G. Dresselhaus, Phys. Rev. **100**, 580 (1955).
- [9] G. Engels, J. Lange, T. Schäpers, and H. Lüth, Phys. Rev. B **55**, R1958 (1997).
- [10] J. Nitta, T. Akazaki, H. Takayanagi, and T. Enoki, Phys. Rev. Lett. **78**, 1335 (1997).
- [11] J. P. Heida, B. J. van Wees, J. J. Kuipers, T. M. Klapwijk, and G. Borghs, Phys. Rev. B **57**, 11911 (1998).
- [12] J.-i. Inoue, G. E. W. Bauer, and L. W. Molenkamp, Phys. Rev. B **70**, 041303 (2004).
- [13] O. V. Dimitrova, arXiv preprint cond-mat/0405339 (2004).
- [14] S. Murakami, Phys. Rev. B **69**, 241202 (2004).
- [15] J. Schliemann and D. Loss, Phys. Rev. B **71**, 085308 (2005).
- [16] B. Das, S. Datta, and R. Reifenberger, Phys. Rev. B **41**, 8278 (1990).
- [17] X. F. Wang and P. Vasilopoulos, Phys. Rev. B **67**, 085313 (2003).
- [18] S. F. Islam and T. K. Ghosh, Journal of Physics: Condensed Matter **24**, 035302 (2011).
- [19] A. Mawrie, T. Biswas, and T. K. Ghosh, Journal of Physics: Condensed Matter **26**, 405301 (2014).
- [20] A. Mawrie, S. Verma, and T. K. Ghosh, Journal of Physics: Condensed Matter **29**, 465303 (2017).
- [21] A. Faridi, R. Asgari, and A. Langari, Phys. Rev. B **98**, 155442 (2018).
- [22] H. Liu, E. Marcellina, A. R. Hamilton, and D. Culcer, Phys. Rev. Lett. **121**, 087701 (2018).
- [23] E. Marcellina, P. Bhalla, A. R. Hamilton, and D. Culcer, Phys. Rev. B **101**, 121302 (2020).
- [24] E. Marcellina, A. Srinivasan, D. S. Miserev, A. F. Croxall, D. A. Ritchie, I. Farrer, O. P. Sushkov, D. Culcer, and A. R. Hamilton, Phys. Rev. Lett. **121**, 077701 (2018).
- [25] J. H. Cullen, P. Bhalla, E. Marcellina, A. R. Hamilton, and D. Culcer, arXiv preprint arXiv:2011.09481 (2020).
- [26] L. Zhu, L. Zhu, M. Sui, D. C. Ralph, and R. A. Buhrman, Science Advances **5**, 10.1126/sciadv.aav8025 (2019).
- [27] Y. Yen and G.-Y. Guo, Phys. Rev. B **101**, 064430 (2020).
- [28] P. C. Lou, A. Katailaha, R. G. Bhardwaj, T. Bhowmick, W. P. Beyermann, R. K. Lake, and S. Kumar, Phys. Rev. B **101**, 094435 (2020).
- [29] C. L. Kane and E. J. Mele, Phys. Rev. Lett. **95**, 226801 (2005).
- [30] M. Ezawa, Phys. Rev. Lett. **109**, 055502 (2012).
- [31] S.-Q. Shen, M. Ma, X. C. Xie, and F. C. Zhang, Phys. Rev. Lett. **92**, 256603 (2004).
- [32] T. Ma and Q. Liu, Applied Physics Letters **89**, 112102 (2006).
- [33] A. Bhattacharya and S. F. Islam, Phys. Rev. B **104**, L081411 (2021).
- [34] F. Mireles and G. Kirczenow, Phys. Rev. B **64**, 024426 (2001).
- [35] C. P. Moca and D. C. Marinescu, Phys. Rev. B **72**, 165335 (2005).
- [36] S. F. Islam, P. Dutta, A. M. Jayannavar, and A. Saha, Phys. Rev. B **97**, 235424 (2018).
- [37] P. Dutta, S. K. Maiti, and S. N. Karmakar, Journal of Applied Physics **114**, 034306 (2013).
- [38] S. K. Maiti, Journal of Applied Physics **110**, 064306 (2011).
- [39] M. Nagano, A. Kodama, T. Shishidou, and T. Oguchi, Journal of physics. Condensed matter : an Institute of Physics journal **21**, 064239 (2009).
- [40] A. Nuber, M. Higashiguchi, F. Forster, P. Blaha, K. Shimada, and F. Reinert, Phys. Rev. B **78**, 195412 (2008).
- [41] M. P. L. Sancho, J. M. L. Sancho, J. M. L. Sancho, and J. R. Rubio, Journal of Physics F: Metal Physics **14**, 1205 (1984).
- [42] M. P. L. Sancho, J. M. L. Sancho, J. M. L. Sancho, and J. R. Rubio, Journal of Physics F: Metal Physics **15**, 851 (1985).
- [43] C. Caroli, R. Combescot, P. Nozieres, and D. Saint-James, Journal of Physics C: Solid State Physics **4**, 916 (1971).
- [44] R. Landauer, The Philosophical Magazine: A Journal of Theoretical Experimental and Applied Physics **21**, 863 (1970).
- [45] M. Büttiker, Phys. Rev. Lett. **57**, 1761 (1986).